PNAS RESEARCH ARTICLE | MEDICAL SCIENCES OPEN ACCESS

A cholesterol-binding bacterial toxin provides a strategy for identifying a specific Scap inhibitor that blocks lipid synthesis in animal cells

Shimeng Xu[a], Jared C. Smothers[a], Daphne Rye[a], Shreya Endapally[a], Hong Chen[b], Shili Li[a], Guosheng Liang[a], Maia Kinnebrew[c,d], Rajat Rohatgi[c,d], Bruce A. Posner[b], and Arun Radhakrishnan[a,1]

Edited by Gerald Shulman, Yale University, New Haven, CT; received October 17, 2023; accepted December 15, 2023

Lipid synthesis is regulated by the actions of Scap, a polytopic membrane protein that binds cholesterol in membranes of the endoplasmic reticulum (ER). When ER cholesterol levels are low, Scap activates SREBPs, transcription factors that upregulate genes for synthesis of cholesterol, fatty acids, and triglycerides. When ER cholesterol levels rise, the sterol binds to Scap, triggering conformational changes that prevent activation of SREBPs and halting synthesis of lipids. To achieve a molecular understanding of how cholesterol regulates the Scap/SREBP machine and to identify therapeutics for dysregulated lipid metabolism, cholesterol-mimetic compounds that specifically bind and inhibit Scap are needed. To accomplish this goal, we focused on Anthrolysin O (ALO), a pore-forming bacterial toxin that binds cholesterol with a specificity and sensitivity that is uncannily similar to Scap. We reasoned that a small molecule that would bind and inhibit ALO might also inhibit Scap. High-throughput screening of a ~300,000-compound library for ALO-binding unearthed one molecule, termed UT-59, which binds to Scap's cholesterol-binding site. Upon binding, UT-59 triggers the same conformation changes in Scap as those induced by cholesterol and blocks activation of SREBPs and lipogenesis in cultured cells. UT-59 also inhibits SREBP activation in the mouse liver. Unlike five previously reported inhibitors of SREBP activation, UT-59 is the only one that acts specifically by binding to Scap's cholesterol-binding site. Our approach to identify specific Scap inhibitors such as UT-59 holds great promise in developing therapeutic leads for human diseases stemming from elevated SREBP activation, such as fatty liver and certain cancers.

SREBP | anthrolysin O | ER–Golgi transport | hemolysis

Significance

Abnormal elevation of lipid synthesis underlies many human diseases, including fatty liver disease and certain cancers. Normal control of lipid synthesis is orchestrated by Scap, a cholesterol-binding membrane protein that regulates activation of SREBPs, transcription factors that upregulate genes for the synthesis of cholesterol, fatty acids, and triglycerides. To reduce lipid synthesis, we sought to develop a specific inhibitor of Scap. Using an unconventional screening strategy based on the striking similarities between Scap and a cholesterol-binding bacterial toxin, we identified a small molecule, called UT-59, that binds to Scap's cholesterol-binding site, thereby blocking SREBP activation and halting lipid synthesis. UT-59 and other compounds identified using this approach are promising leads to develop therapies for fatty liver and certain cancers.

The molecular machinery that ensures lipid homeostasis in animal cells consists of two key protein components. The first component is a family of membrane-bound transcription factors called sterol regulatory element-binding proteins (SREBPs), which are attached to the endoplasmic reticulum (ER) membrane through two transmembrane (TM) helices and control the expression of lipogenic genes (1, 2). The SREBP family consists of three isoforms—SREBP-1a, SREBP-1c, and SREBP-2—that have distinct yet overlapping specificities for upregulation of genes. The SREBP-1a isoform activates genes encoding enzymes that produce fatty acids, triglycerides, and cholesterol. The SREBP-1c and SREBP-2 isoforms have more specialized specificities, with SREBP-1c primarily activating the genes for fatty acid and triglyceride production and SREBP-2 primarily activating genes for cholesterol production as well as the LDL receptor. All three SREBP isoforms bind to the second key component of the lipid homeostatic machinery, a cholesterol-sensing membrane protein called Scap, which regulates the activation of the SREBPs (3).

Scap is embedded in ER membranes through eight TM helices that are connected by seven loops (see schematic in *SI Appendix*, Fig. S1). Two of these loops, Loop 1 (L1, ~240 amino acids) and Loop 7 (L7, ~175 amino acids), are large domains that project into the lumen of the ER where they bind each other (4–7). When ER cholesterol levels are low, a hexapeptide on Scap's cytosolic Loop 6 becomes exposed and provides a binding site for the coat protein complex II (COPII), which clusters the Scap/SREBP complex into coated vesicles for transport to the Golgi apparatus. In the Golgi, two proteases, Site-1 protease (S1P) and Site-2 protease (S2P), sequentially cleave the SREBPs (Fig. 1 *A*, *Left*). This dual cleavage releases the transcription factor domains of SREBPs from the membrane into the cytosol, from where they travel to the nucleus and activate lipogenic genes. As a result, cellular levels of cholesterol, as well as those of fatty acids and triglycerides, increase. When cholesterol levels in the ER rise above a threshold, the sterol binds to Scap's L1 domain and changes Scap's conformation. The cholesterol-bound Scap then binds to one of two ER membrane retention proteins, Insig-1 or Insig-2 (Fig. 1 *A*, *Right*), which blocks COPII

Author contributions: S.X., G.L., R.R., B.A.P., and A.R. designed research; S.X., J.C.S., D.R., S.E., H.C., S.L., M.K., and A.R. performed research; S.X., J.C.S., and A.R. contributed new reagents/analytic tools; S.X., J.C.S., D.R., S.E., H.C., S.L., G.L., M.K., R.R., B.A.P., and A.R. analyzed data; and S.X. and A.R. wrote the paper.

The authors declare no competing interest.

This article is a PNAS Direct Submission.

[1]To whom correspondence may be addressed. Email: arun.radhakrishnan@utsouthwestern.edu.

This article contains supporting information online at https://www.pnas.org/lookup/suppl/doi:10.1073/pnas.2318024121/-/DCSupplemental.

Published February 8, 2024.

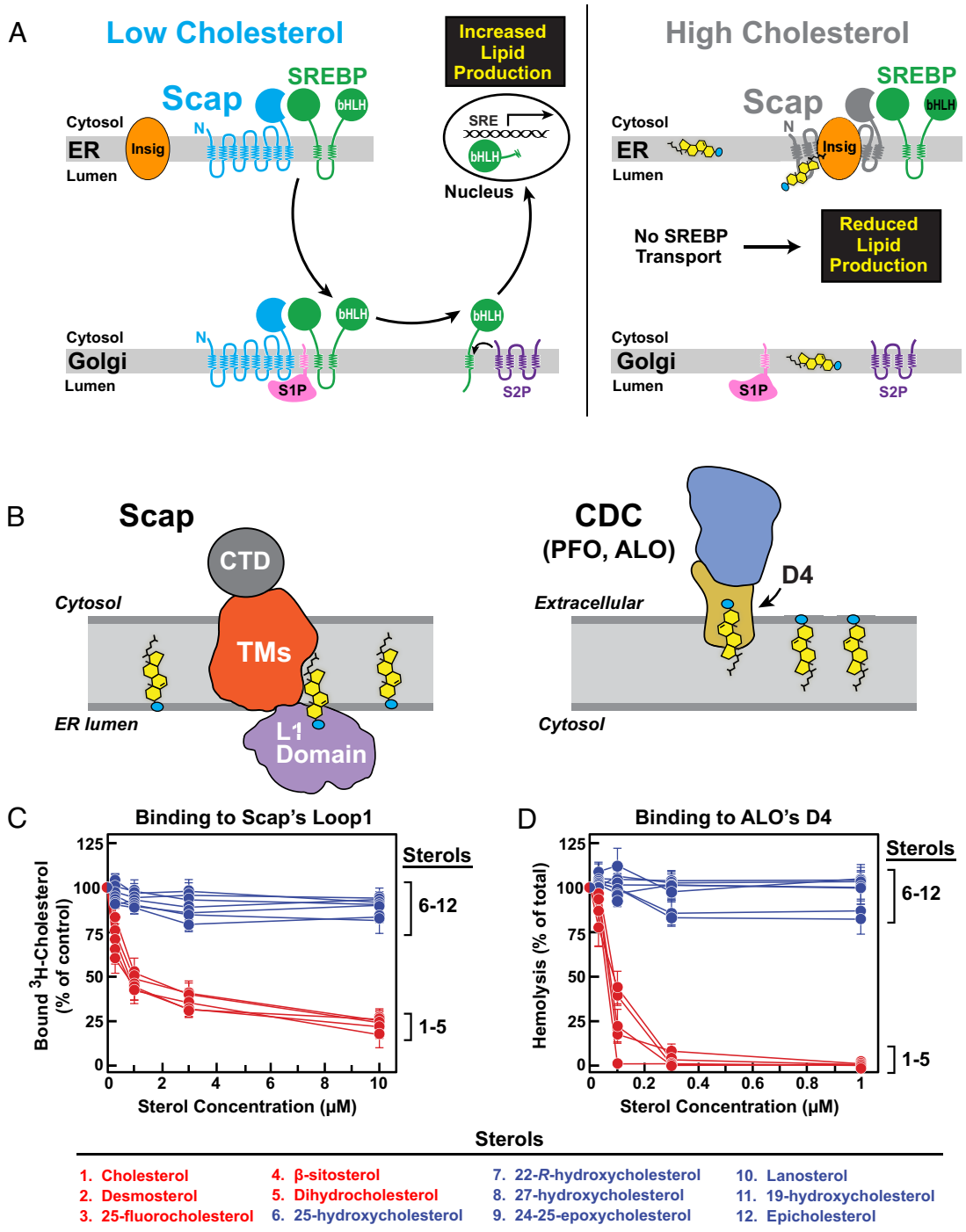

Fig. 1. Scap, the cholesterol sensor that controls SREBP activation, shares identical sterol binding specificity with ALO, a bacterial toxin that forms membrane pores. (*A*) Overview of the SREBP pathway. (*Left*) When cellular cholesterol levels are low, Scap escorts SREBPs from ER to Golgi, where two proteases (S1P and S2P) sequentially cleave the SREBPs, releasing their bHLH transcription factor domains that then travel to the nucleus and activate genes involved in lipid production. (*Right*) When cholesterol levels rise above a threshold concentration, the sterol binds to Scap and changes Scap's conformation to promote binding to Insigs, which retain Scap in the ER. As a result, transport of SREBPs to the Golgi is halted, thus reducing transcriptional activation of lipogenic genes. (*B*) Structure-based models of Scap and ALO. (*Left*) Scap is a polytopic membrane protein that can be divided into three domains—i) a luminal domain (purple) composed of an intertwined complex of Loop1 (L1) with Loop7 (L7) that contains a cholesterol-binding site in L1; ii) a transmembrane domain (red) that binds Insigs when cholesterol is bound to L1; and iii) a cytosolic domain (gray) that binds SREBPs regardless of whether L1 is bound to cholesterol or not. (*Right*) ALO is a soluble protein that harbors a cholesterol-binding site in its Domain 4 (D4, gold). The remainder of the ALO protein (blue) facilitates its oligomerization once cholesterol is bound to D4. (*C*) Competitive binding of unlabeled sterols to His_6-Scap(L1)-FLAG. Each reaction, in a final volume of 200 μL of buffer A with 0.004% NP-40 and 0.002% FC-13, contained 0.2 μg of His_6-Scap(L1)-FLAG, 1 μg of BSA, 150 nM [^{3}H]cholesterol (110,000 dpm/pmol), and varying concentrations of the indicated unlabeled sterol. After incubation for 4 h at 4 °C, bound [^{3}H]cholesterol was measured as described in *SI Appendix, Methods*. The 100% control value, determined in the absence of competitor, was 544 fmol/tube. (*D*) Sterol specificity for inhibition of hemolysis by His_6-ALO. Each reaction, in a final volume of 50 μL of buffer A, contained 1 nM of His_6-ALO and varying amounts of the indicated sterols solubilized in DMSO [final concentration of DMSO in each reaction tube was 4% (v/v)]. After incubation for 1 h at room temperature, 450 μL of rabbit erythrocytes (isolated and resuspended in buffer C as described in *SI Appendix, Methods*) was added to each reaction mixture. After incubation for 10 min at room temperature, the extent of hemolysis was quantified as described in *SI Appendix, Methods* by measuring the release of hemoglobin (absorbance at 540 nm). The amount of hemoglobin released after treatment with 1% (w/v) Triton X-100 detergent was set to 100%, and all values were normalized to this set-point. (*C* and *D*) Each data point represents the average of three assays and error bars represent the SE. When not visible, error bars are smaller than the size of the symbols.

binding to Scap. As a result, transport of the Scap/SREBP complex to the Golgi is halted, and lipid synthesis declines. Through this negative feedback mechanism orchestrated by small changes in ER cholesterol levels, the Scap/SREBP machinery ensures optimal supply of lipids for membrane assembly while guarding against lipid overaccumulation (8).

In certain pathological situations, the Scap/SREBP regulatory system fails to protect against lipid overaccumulation. For instance, in type 2 diabetes, elevated insulin levels lead to hyper-activation of SREBP-1c in the liver by increasing both its transcription as well as its proteolytic processing (9, 10). This in turn results in excessive synthesis of hepatic fatty acids and triglycerides, which can produce hypertriglyceridemia and fatty liver disease (11, 12). Indeed, fatty liver-induced cirrhosis is the leading cause of liver transplantation in the US (12). Inasmuch as the insulin-induced hyper-activation of SREBP-1c requires its ER-to-Golgi transport by Scap, there has been considerable interest in developing small-molecule inhibitors of the Scap/SREBP pathway to prevent fatty liver and hypertriglyceridemia. Such an inhibitor may also be useful in stunting the growth of cancer tumors that use the Scap/SREBP pathway to generate lipids for assembling the membranes of their rapidly proliferating cells (13–15).

The ideal inhibitor for the Scap/SREBP pathway would be one that has minimal effects on general cellular functions, such as ER-to-Golgi transport and the ER stress response. To achieve such specificity, Scap would be the best component to target since its predominant role is to escort SREBPs to Golgi for proteolytic activation. In contrast, inhibition of other pathway components (Fig. 1*A*), such as S1P, S2P, or the molecules involved in assembly of COPII vesicles, would result in unwanted side effects since they mediate many cellular processes other than activation of SREBPs (16–20). Indeed, small molecules reported by other groups as inhibitors of the Scap/SREBP pathway suffer from a lack of specificity, as discussed below.

One group used a cell morphology profiling assay to screen a chemical library for compounds that inhibited insulin-induced differentiation of adipocytes (21). One of their hits blocked ER-to-Golgi transport of Scap/SREBP and was named fatostatin. However, the specificity of fatostatin for Scap was not tested in direct binding assays (22), and a later study showed that fatostatin inhibited cell growth in a Scap-independent manner (23). Two other groups screened for Scap inhibitors by adding chemical libraries to cultured cells that were engineered to express a reporter protein under control of an SREBP-dependent promoter (24, 25). However, one of the compounds identified, xanthohumol, bound to COPII proteins (24). The other compound, betulin, was not rigorously evaluated for interaction with Scap's cholesterol-binding site (25), and a later study showed that betulin inhibited the mTOR signaling pathway (26). Another group used a cellular thermal shift assay to screen a chemical library for compounds that increased the thermal stability of Scap (27) and found a compound, lycorine, that causes the degradation of Scap; however, its specificity for Scap's cholesterol-binding site was not rigorously tested. Yet another group reported that dipyridamole, an FDA-approved phosphodiesterase inhibitor that decreases platelet aggregation, also inhibited ER-to-Golgi transport of Scap (28). However, this study did not report any test of dipyridamole's direct interaction with Scap's cholesterol-binding site. Thus, to date, there have been no reports of a specific inhibitor of Scap that inhibits SREBP processing without affecting other pathways.

In the current studies, we describe a method for large-scale, high-throughput screening for Scap inhibitors. The method is based on our finding of a striking similarity in how Scap's extramembranous L1 domain dips into the ER membrane to bind cholesterol and how Anthrolysin O (ALO), a cholesterol-binding soluble bacterial toxin (29), dips into the plasma membrane to bind cholesterol and form pores. Based on this similarity, we show that ALO can be used as a surrogate for Scap's L1 to identify non-sterol molecules that occupy the cholesterol-binding site. Unlike Scap, ALO is a stable cholesterol-binding protein that can be produced in large quantities and is amenable to screening assays for identifying small molecules that bind ALO. High-throughput screening of a ~300,000-compound library identified one ALO-binding molecule, designated as UT-59, that specifically bound Scap at its cholesterol-binding site in L1. This interaction changed Scap's conformation to promote its binding to Insigs, and blocked transport of the Scap/SREBP complex from ER to Golgi to abolish SREBP cleavage in cultured human cells as well as in the mouse liver. UT-59 promises to be a useful resource to 1) study the molecular mechanism of how cholesterol inhibits Scap; 2) determine the sensitivity of cancer cell lines to inhibition of the Scap/SREBP pathway; and 3) begin to test the effects of pharmacologically blocking the synthesis of cholesterol, fatty acids, and triglycerides in animal models of lipid dysregulation.

Results

ALO and Scap Share Identical Sterol Specificity. Our assay for Scap inhibitors takes advantage of cholesterol-dependent cytolysins (CDCs), a family of bacterial toxins that bind cholesterol and form pores to lyse membranes (30). Of the more than 25 members of this family, we have focused on Perfringolysin O (PFO) and ALO, two CDCs that are secreted as soluble proteins by *Clostridium perfringens* and *Bacillus anthracis*, respectively (29, 31). Both toxins bind to cholesterol in animal cell membranes. Upon binding, the proteins form circular oligomers, creating pores that kill the cell. When added to artificial membrane bilayers that contain varying amounts of cholesterol, the toxins bind in a non-linear fashion. Binding is low until cholesterol reaches a threshold concentration, whereupon binding increases exponentially (32–34). This finding intrigued us because we had previously found that cholesterol inhibition of Scap/SREBP transport also shows a threshold response to ER membrane cholesterol content (8). SREBP processing persisted as long as the cholesterol content of ER membranes was below 5 mol% of total ER membrane lipids. When cholesterol exceeded this threshold concentration, SREBP transport was abruptly inhibited. Inasmuch as inhibition of SREBP processing requires cholesterol binding to Scap, we reasoned that Scap binds cholesterol only when it exceeds 5 mol% of lipids in ER membranes (8, 35). We then wondered whether CDC binding to ER membranes would also show a threshold at 5 mol% cholesterol. Indeed, we found this to be the case. PFO, one of the two CDCs that we have studied, bound to purified ER membranes with a sharp threshold at 5 mol% cholesterol, correlating perfectly with inhibition of SREBP processing (33).

We began to suspect that this common sensitivity of soluble PFO and membrane-bound Scap for ER cholesterol may be more than just a coincidence when a series of subsequent studies showed that the cholesterol-binding site in Scap is localized in its L1 domain (36) that projects out of the membrane into the ER lumen where it binds to L7 (4, 7). We speculated that Scap's cholesterol-sensing L1 domain may detect a pool of cholesterol that is accessible at membrane surfaces in the same manner as the cholesterol-sensing domain 4 (D4) of CDCs (Fig. 1*B*) (34). To further understand these different cholesterol-sensing domains, we compared their specificity for structural features of cholesterol. For these assays, we overexpressed L1 of hamster Scap (residues 46 to 269) with a His_6-tag near its NH_2-terminus and a 3×FLAG

tag at its COOH-terminus in mammalian HEK293S GNTI$^-$ cells. The resulting recombinant protein, designated as His_6-Scap(L1)-FLAG, was purified as described in *SI Appendix*, *Methods*. We also overexpressed ALO with a His_6-tag at its NH_2-terminus in bacterial cells, and the resulting recombinant protein, designated as His_6-ALO, was purified as described in *SI Appendix*, *Methods*. We used ALO instead of PFO in these assays because ALO is easier to purify in large quantities and is more stable than PFO. We have previously shown that the cholesterol-sensing D4 domains of PFO and ALO share an identical threshold sensitivity for membrane cholesterol (34). Gel filtration chromatography of both purified proteins, His_6-Scap(L1)-FLAG and His_6-ALO, showed that they eluted as single peaks (*SI Appendix*, Fig. S2 *A* and *B*, *Left*) and their homogeneity was verified by Coomassie staining (*SI Appendix*, Fig. S2 *A* and *B*, *Right*). We then assayed for the ability of 12 sterols with diverse structures to bind to these purified proteins. For His_6-Scap(L1)-FLAG, we adapted previously described competition assays (4, 36) to measure the ability of the 12 sterols to compete with [^{3}H]cholesterol for binding to the protein (Fig. 1*C*). To measure the binding of sterols to His_6-ALO, we assayed their effects on hemolysis by His_6-ALO. When incubated with red blood cells (RBCs), His_6-ALO binds to cholesterol in the membrane, forming pores that lyse the cell, releasing hemoglobin. When the His_6-ALO was preincubated with cholesterol, the sterol occupied the binding pocket, preventing ALO from binding to the membrane and inhibiting hemolysis. We used this hemolysis inhibition assay to explore ALO's binding specificity for the 12 sterols (Fig. 1*D*).

A comparison of the results in Fig. 1 *C* and *D* reveals that the sterol specificity for binding to Scap's L1 is identical to that of ALO. As expected, both Scap and ALO bind cholesterol. In addition, both Scap and ALO bind desmosterol, 25-fluorocholesterol, and β-sitosterol, which have an extra double bond, a fluorine group, and an ethyl group on their side chains, respectively, as well as dihydrocholesterol, where the double bond in the steroid nucleus is reduced (red curves, #1 to 5). Upon binding Scap, these four sterols trigger the same conformational change as induced by cholesterol (37) and block SREBP processing. However, sterol derivatives with an additional hydroxyl or epoxy group on the iso-octyl side chain, such as 25-hydroxycholesterol (25HC), do not bind to ALO or Scap (blue curves, #6 to 9). While they do not bind Scap, 25HC and other side-chain oxysterols block SREBP processing by binding to Insig, promoting Insig/Scap complex formation and triggering the same conformational change in Scap as induced by cholesterol (38, 39). Other sterol derivatives, including the biosynthetic precursor lanosterol, 19-hydroxycholesterol, or epicholesterol, which do not block SREBP processing, do not bind to ALO or to Scap (blue curves, #10 to 12). The shared ability of Scap and ALO to distinguish between cholesterol and epicholesterol, a diastereomer differing only in the orientation of the sterol 3-hydroxyl group, suggests that the binding pockets of ALO and Scap may be similar even though there is no sequence resemblance. This similarity raised the possibility that ALO could be used as a surrogate for Scap to identify non-sterol molecules that occupy the cholesterol-binding site and prevent SREBP processing.

Screening for ALO Binders Identifies UT-59, Which Specifically Blocks SREBP Processing. We adapted the hemolysis assay described above as a primary screen for ALO-binding compounds in a high-throughput format involving 384-well microtiter plates (scheme shown in Fig. 2*A*). The *Left* panel of Fig. 2*B* shows an experiment designed to validate the microtiter plate assay (*SI Appendix*, *Methods*) for inhibition of ALO-induced hemolysis by cholesterol. As expected, ALO caused complete hemolysis (column 1), and DMSO addition (control) had no effect (column 2). In contrast, cholesterol added in DMSO blocked hemolysis completely (column 3), whereas epicholesterol had no effect (column 4). When tested in 48-replicate wells, the all-or-none response to cholesterol led to a statistical Z-score of 0.88, which indicates that variability of the assay is low enough to permit robust screening of candidate compounds (40). The *Right* panel of Fig. 2*B* shows a photograph of a section of the 384-well plate with 16 of the 48 replicates for each of the conditions, illustrating the robust all-or-none response to cholesterol in a visual manner.

Armed with this simple high-throughput screening assay, we screened the chemical library available through the High-Throughput Screening Core facility at our institution (details about this library can be found at https://www.utsouthwestern.edu/research/core-facilities/high-throughput-screening/libraries/). A total of 293,918 compounds were tested at a concentration of 6 μM for inhibition of ALO-induced hemolysis and the compounds were ranked by their R_z scores (41), a statistical score reflecting the number of SDs a library compound's activity is from the mean compound effect on hemolysis (Fig. 2*C*). We applied a cut-off at a R_z score <= −3 (reflecting 3 or more SDs from the mean), which identified 853 candidate compounds that significantly inhibited ALO-induced hemolysis (dashed line in Fig. 2*C*).

Fig. 2*D* shows a flowchart that summarizes how we winnowed down the 853 candidate compounds to identify a specific Scap inhibitor. We used immunoblot analysis to test each of the 853 hits for their ability to inhibit ER-to-Golgi transport and cleavage of SREBP1 and SREBP2 when added in DMSO solutions (at concentrations of 14, 40, and 120 μM) to sterol-depleted SV-589 human fibroblast cells in culture (secondary screen, schematic shown in Fig. 2*A*). 28 of the 853 hits suppressed SREBP1 and SREBP2 processing by >50% when they were incubated with the cells for 3 h at a concentration of 40 μM. We subjected each of these 28 candidates to a counter-screen for nonspecific inhibition of ER-to-Golgi transport (counter screen 1, schematic shown in Fig. 2*A*). For this purpose, we used a previously described mutant cell line that expresses a truncated form of S1P lacking its single TM helix (Fig. 1*A*) (42). The truncated S1P, designated as S1P(ΔTM), undergoes autocatalytic cleavage in the ER and the mature form travels to the Golgi. Without a TM helix to anchor it in the Golgi membrane, S1P(ΔTM) is secreted (43). Unlike ER-to-Golgi transport of Scap, transport of S1P(ΔTM) is insensitive to cellular sterol levels (43). Of the 28 remaining candidates, 24 of them inhibited the secretion of S1P(ΔTM) when they were incubated with the cells for 4 h at a concentration of 10 μM, suggesting that they were blocking ER-to-Golgi transport in a non-specific fashion and were removed from further consideration.

The remaining four candidates were subjected to an additional counter-screen for non-specific inhibition of any one of the steps of ER-to-Golgi transport, S1P cleavage, or S2P cleavage (counter screen 2, schematic shown in Fig. 2*A*). For this test, we studied the transport of ATF6, which is a transcription factor synthesized as an ER membrane-bound precursor that must be transported to the Golgi for processing by S1P and S2P, just like the SREBPs (16). However, in contrast to SREBPs whose transport is triggered by the lack of cholesterol, the transport of ATF6 is triggered by accumulation of unfolded proteins in the ER which causes ER stress. Such ER stress can be triggered by treatment of cells with thapsigargin, which depletes the ER of calcium (16). Two of the four remaining candidates inhibited the thapsigargin-induced transport and processing of ATF6 when incubated with cells for 4 h at a concentration of 10 μM, suggesting that they were either blocking

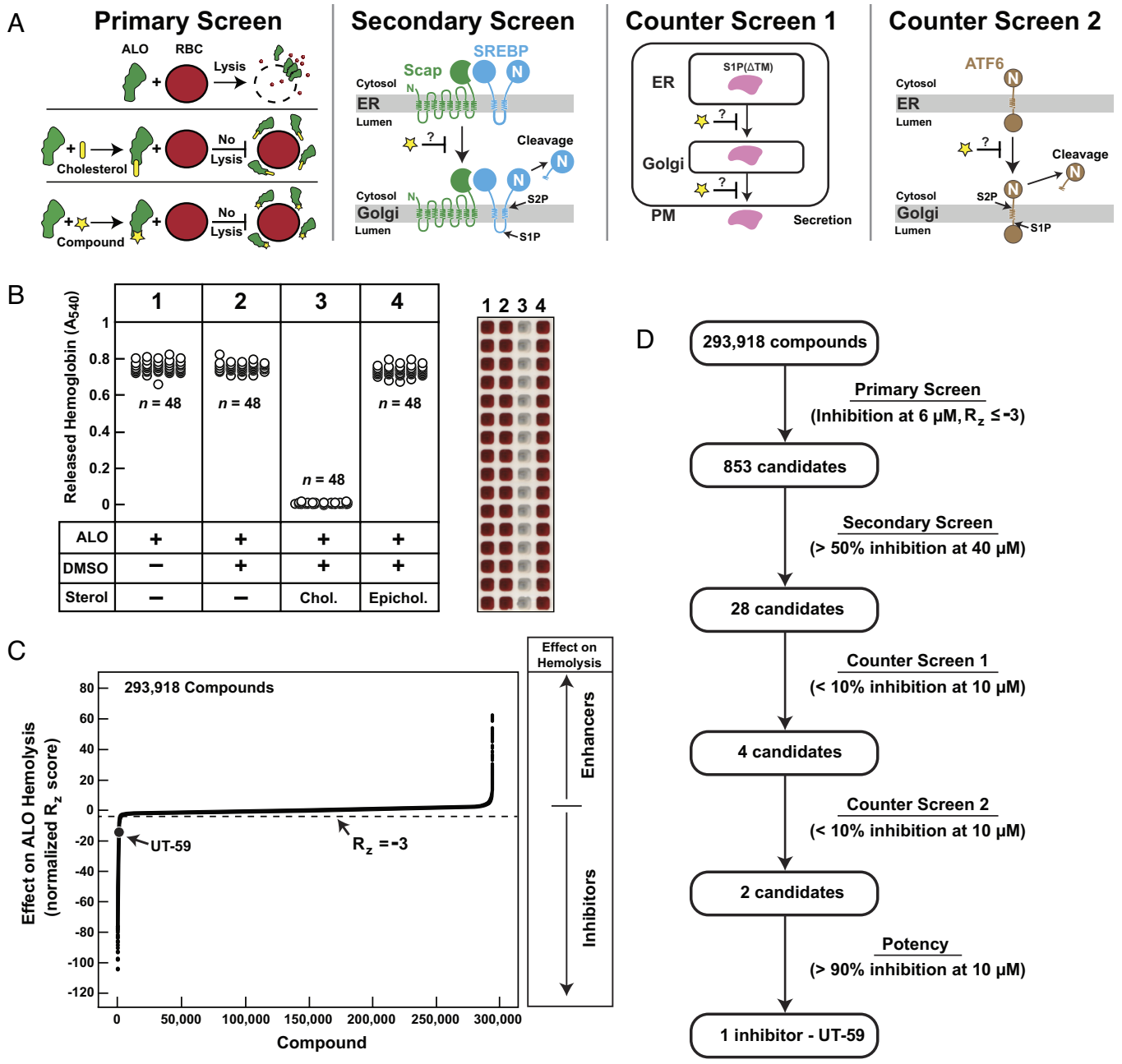

Fig. 2. High-throughput screening identifies UT-59 as a candidate inhibitor of SREBP processing. (*A*) Schematic diagrams of screens to evaluate candidate compounds (yellow star) for their ability to inhibit Scap in a specific manner. The primary screen tested the ability of compounds to inhibit lysis of rabbit red blood cells (RBCs) by ALO, a cholesterol-binding toxin. Potent candidate inhibitors from the primary screen were then evaluated in a secondary screen for their ability to block the proteolytic cleavage of SREBP1 and SREBP2 in cholesterol-depleted SV589 cells. Candidate compounds that emerged from the primary and secondary screens were then evaluated for their specificity in two counter screens that assessed whether these compounds i) blocked the ER-to-Golgi transport and subsequent secretion of a model protein, S1P(ΔTM), a process that does not depend on Scap or cholesterol, or ii) blocked the thapsigargin-induced proteolytic cleavage of ATF6, a transcription factor that is transported from ER to Golgi like the SREBPs but in a manner that also does not depend on Scap or cholesterol. (*B*) Robustness of the primary screen assay for high-throughput screening. Each reaction, in a single well of a 384-well plate, was comprised of 25 μL of buffer C containing 3 nM of His_6-ALO without or with supplementation of 0.3 μL of DMSO containing 6 μM of the indicated sterol. After incubation for 1 h at room temperature, 45 μL of rabbit RBCs, resuspended in buffer C as described in *SI Appendix, Methods*, were added to each well. Following incubation for 20 min at room temperature, the extent of hemolysis was assessed as described in *SI Appendix, Methods* by measuring the release of hemoglobin (absorbance at 540 nm). Analysis of 48 replicate wells of each condition indicates an all-or-none inhibition of ALO-induced hemolysis by cholesterol. The image on the *Right* shows a section of the 384-well plate with 16 of the 48 replicates for each condition, illustrating the robust all-or-none response to cholesterol in a visual manner. Chol., cholesterol; Epichol., epicholesterol. (*C*) Rank ordering of compounds by their ability to inhibit ALO-induced hemolysis. High-throughput screening of 293,918 compounds at a concentration of 6 μM identified 853 candidates that significantly reduced ALO-induced hemolysis in the primary screen [3 or more SDs from the mean of the population ($R_z \leq -3$), dashed line]. (*D*) Flowchart summary of screen results. The 853 candidates identified through the primary screen (*C*) were subjected to secondary and counter screens, leading to elimination of all but one compound that we designated as UT-59 [black circle in (*C*)].

ER-to-Golgi transport in a manner independent of Scap or inhibiting the activity of S1P or S2P. These two candidates were removed from further consideration. Of the two remaining candidates, the most potent one, ethyl 4-({[4-(5-cyclobutyl-1,2,4-oxadiazol-3-yl) anilino] carbonyl} amino) benzoate, was chosen for further study and named UT-59 (Fig. 2*D*). While UT-59 was not the most potent inhibitor of ALO-induced hemolysis in the primary screen (black circle, Fig. 2*C*), it was the only ALO-binding molecule that passed the stringent secondary and counter screens for specific inhibition of SREBP transport and processing.

We next obtained fresh batches of UT-59 (chemical structure and comparison to cholesterol shown in Fig. 3*A*) and carried out detailed analysis to verify its performance in the primary, secondary, and counter screens. In the hemolysis inhibition assay (primary screen), dose curve analysis showed that UT-59 bound to ALO and inhibited hemolysis by ~80% at concentrations of ~3 μM (Fig. 3*B*). In comparison, cholesterol inhibited hemolysis at 10-fold lower concentrations, whereas epicholesterol and 25HC, two sterols that we had previously shown to not bind ALO (Fig. 1*D*), did not affect hemolysis at the highest concentrations tested. We then added UT-59 to sterol-depleted human fibroblasts and analyzed SREBP cleavage by immunoblot analysis (secondary screen). Detailed dose curves showed that UT-59 suppressed the processing of both SREBP1 and SREBP2 at concentrations of ~3 μM (lane 4 in the *Top* two panels, Fig. 3*C*). We then assessed the effects of UT-59 on secretion of S1P(ΔTM) (counter screen 1). As shown in Fig. 3*D*, UT-59 did not reduce S1P(ΔTM) secretion, even at concentrations as high as 30 μM (lanes 1 to 6). Brefeldin A, a known inhibitor of transport between the ER and Golgi (44), completely blocked secretion of S1P(ΔTM) (lane 7), whereas 25HC and cholesterol had no effect (lanes 8 and 9). Finally, we tested the effects of UT-59 on the thapsigargin-induced transport and processing of ATF6 (counter screen 2). In this experiment, we transfected human fibroblasts with HSV-tagged ATF6 and then induced its cleavage by treatment with thapsigargin (lanes 1 and 2, Fig. 3*E*). When we co-incubated the cells with thapsigargin and 30 μM of UT-59 (lane 3, Fig. 3*E*), cleavage of ATF6 persisted, suggesting that UT-59 did not block thapsigargin-induced ATF6 processing at this concentration. As expected, incubation with cholesterol also did not block thapsigargin-induced ATF6 processing (lane 4, Fig. 3*E*). Together, these experiments confirm the results of our high-throughput screen and establish UT-59 as a promising candidate non-sterol small molecule that specifically suppresses the ER-to-Golgi transport of SREBPs in a manner similar to cholesterol.

To determine whether UT-59-induced suppression of SREBP processing led to downregulation of target genes, we isolated total RNA from human fibroblasts treated with UT-59 and measured mRNA levels by quantitative real-time PCR. As expected from the reduction in SREBP cleavage observed in the immunoblot analysis (Fig. 3*C*), UT-59 dramatically reduced mRNAs of target genes of SREBP1 (Insig-1, ACSS2, ACC1, FASN, SCD1) and SREBP-2 (HMG-CoA synthase, HMG-CoA reductase, LDL receptor, PCSK9, and others) (*SI Appendix*, Fig. S3*A*). Such reduction in lipogenic gene mRNA levels would be expected to lead to a decline in lipid synthesis. Indeed, we observed that treatment with UT-59 reduced de novo lipid synthesis, as judged by an ~fivefold decrease in the incorporation of [^{14}C]acetate into lipids (*SI Appendix*, Fig. S3*B*). Thus, UT-59 blocks SREBP processing, lowers mRNA levels of SREBP target genes, and reduces lipid synthesis. UT-59's effects were not restricted to human fibroblasts as a dose of 3 μM inhibited SREBP1 and SREBP2 processing in human colon cells (Caco2), mouse liver cells (Hepa1c1c7), human liver cells (HuH7), and hamster ovary cells (CHO-K1) (lane 5 in all panels, *SI Appendix*, Fig. S4).

We next assessed whether treatment with UT-59 induced cellular toxicity. First, we tested whether UT-59 induced ER stress, as judged by triggering of ATF6 processing in human fibroblasts (*SI Appendix*, Fig. S5*A*). In contrast to treatment with thapsigargin (lanes 1 and 2), treatment with 30 μM of UT-59 did not trigger ATF6 cleavage (*lane 3*). As expected, cholesterol had no effect on induction of ATF6 cleavage (lane 4). Next, we tested the effects of UT-59 on cellular ATP levels, a proxy for cellular viability. Dose curve analysis showed that incubation of human fibroblasts with up to 30 μM of UT-59 for 24 h did not reduce cellular ATP levels, regardless of whether the cells were being grown in lipoprotein-rich serum (FCS) or lipoprotein-deficient serum (LPDS) (*SI Appendix*, Fig. S5*B*). Treatment with 25HC or cholesterol for this same 24-h period also did not affect cellular ATP levels, whereas treatment with camptothecin, an inhibitor of DNA synthesis that triggers cellular apoptosis (45), severely diminished cellular viability (*SI Appendix*, Fig. S5*B*).

While the aforementioned results suggest that UT-59 does not cause short-term toxicity, we wondered whether the UT-59-induced suppression of SREBP processing and subsequent inhibition of lipid synthesis would affect cellular viability over longer time periods. To test this notion, we used CHO-7 cells, a subline of CHO-K1 cells that have adapted to grow in media deficient in lipoproteins (LPDS) (46). In the absence of an exogenous source of cholesterol and other lipids, the CHO-7 cells must rely on SREBP-mediated endogenous lipid synthesis for their survival. Long-term incubation of CHO-7 cells with 25HC, which suppresses the SREBP pathway but cannot substitute for cholesterol as a structural component of cell membranes, results in cell death (47). Inasmuch as UT-59 would also not be expected to substitute for cholesterol to maintain the integrity of cell membranes, we tested whether chronic treatment with UT-59 would suppress SREBPs and starve the cells of lipids leading to cell death. As shown in *SI Appendix*, Fig. S5*C*, UT-59 treatment over a 10-d period killed CHO-7 cells in a dose-dependent manner, similar to what was observed with 25HC. The concentrations of UT-59 that result in complete cell death (3 μM and higher) correspond exactly to the concentrations that suppress SREBP processing in CHO cells (*SI Appendix*, Fig. S4, *Bottom*). If UT-59-induced cell death was due to suppression of SREBPs and reduction in cellular lipids, we would expect the cells to survive if they were provided exogenous lipids. Indeed, UT-59-treated CHO-7 cells survived when they were supplied exogenous mevalonate, cholesterol, and fatty acids (the end-products of the genes activated by SREBP1 and SREBP2) (*SI Appendix*, Fig. S5*D*). Similar cellular survival was observed when exogenous lipids were provided to 25HC-treated CHO-7 cells (*SI Appendix*, Fig. S5*D*). Combined, this set of results suggests that UT-59 is not generally toxic to cells when treated for short times but can affect cellular viability over longer time periods through a reduction in lipid synthesis caused by suppression of SREBP processing.

UT-59 Binds Scap and Promotes Scap/Insig Complex Formation to Retain Scap in ER. We next focused on understanding the molecular mechanism by which UT-59 blocks SREBP processing. Insofar as the screening strategy that unearthed UT-59 was designed to provide a readout of an interaction with the cholesterol-binding site in Scap's L1, we sought to determine whether UT-59 bound to Scap. Using the competition assay described in Fig. 1*C*, we found that UT-59 competed with [^{3}H]cholesterol for binding to His$_6$-Scap(L1)-FLAG to a similar degree as unlabeled cholesterol (Fig. 4*A*). As controls, epicholesterol and 25HC, two sterols that we had previously shown to not bind Scap's L1 (Fig. 1*C*), did not compete for the binding of [^{3}H]cholesterol to His$_6$-Scap(L1)-FLAG (Fig. 4*A*). We next used a previously described trypsin digestion assay (48) to test whether the binding of UT-59 to Scap's L1 caused the same conformational change in Scap as induced by binding of cholesterol. We first depleted CHO-K1 cells of sterols, after which we incubated the cells with either UT-59 or sterols. The cells were then processed to generate sealed membrane vesicles, which were then incubated with trypsin and subjected to immunoblot analysis. A trypsin-protected fragment of Scap was detected with a monoclonal antibody directed against

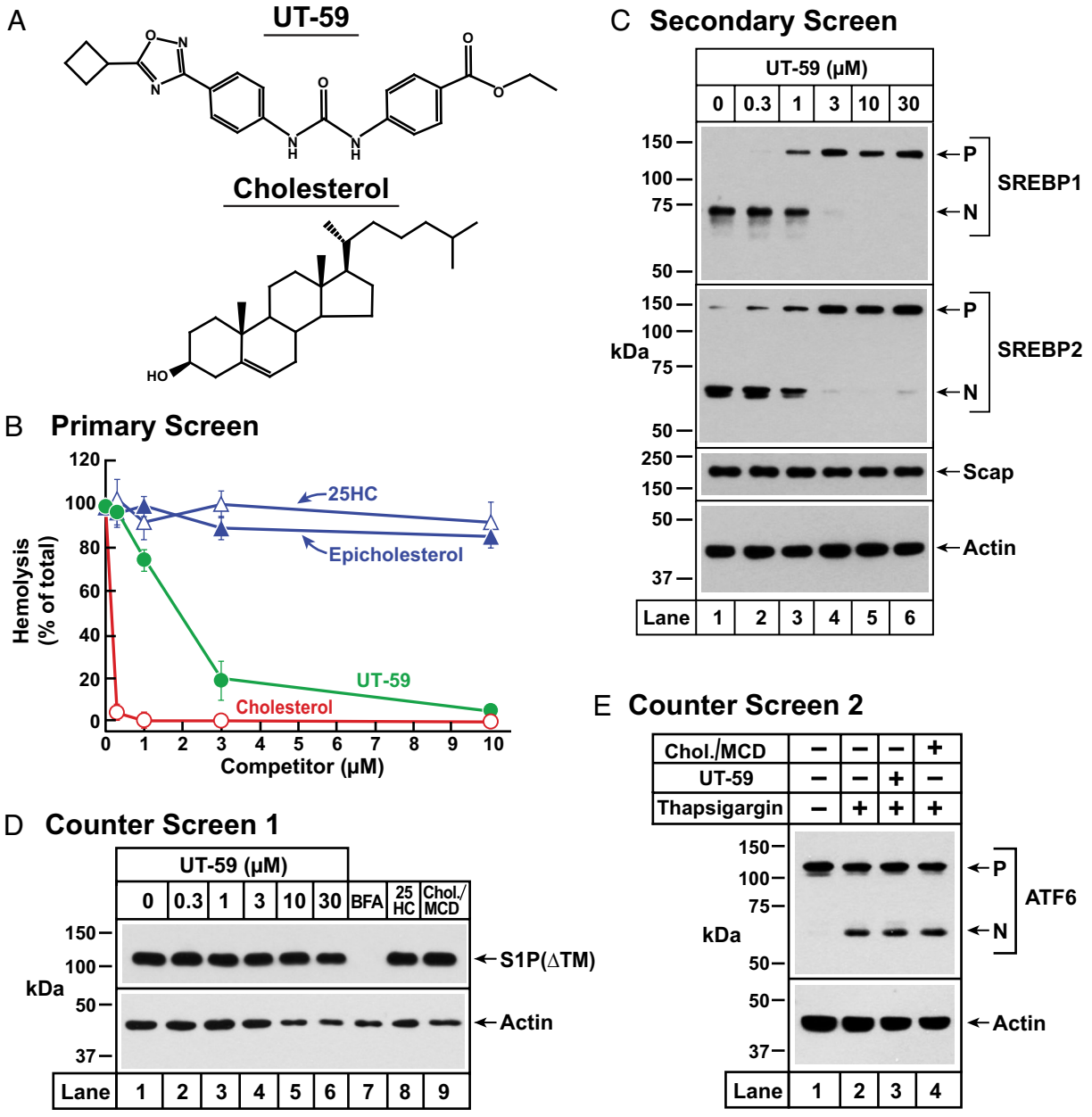

Fig. 3. Properties of UT-59 in primary and secondary screens. (*A*) Chemical structures of UT-59 (molecular weight = 406.44 Da) and cholesterol (molecular weight = 386.65 Da). (*B*) UT-59 inhibits hemolysis by His_6-ALO. Each reaction mixture, in a final volume of 50 μL of buffer A, contained 1 nM of His_6-ALO and varying amounts of UT-59 or the indicated sterols, all solubilized in DMSO [final concentration of DMSO in each reaction was 4% (v/v)]. After incubation for 1 h at room temperature, 450 μL of rabbit erythrocytes (isolated and resuspended in buffer C as described in *SI Appendix, Methods*) was added to each reaction mixture. After incubation for 10 min at room temperature, the extent of hemolysis was quantified as described in *SI Appendix, Methods* by measuring the release of hemoglobin (absorbance at 540 nm). The amount of hemoglobin released after treatment with 1% (w/v) Triton X-100 detergent was set to 100% and all values were normalized to this set-point. Each data point represents the average of three assays and error bars represent the SE. When not visible, error bars are smaller than the size of the symbols. (*C*) UT-59 inhibits proteolytic processing of SREBP1 and SREBP2. On day 0, SV-589 cells were set up in medium B at a density of 4×10^4 cells per well of a 48-well plate. On day 1, the medium was removed, cells were washed twice with 500 μL of PBS followed by addition of 200 μL of cholesterol-depleting medium D. After incubation at 37 °C for 1 h, the medium was removed, cells were washed twice with 500 μL of PBS followed by addition of 200 μL of medium C containing the indicated concentrations of UT-59. After incubation at 37 °C for 3 h, the medium was removed, cells were washed twice with 500 μL of PBS, harvested, and equal aliquots of cell lysates were subjected to immunoblot analysis as described in *SI Appendix, Methods*. *P*, precursor forms of SREBP1 and SREBP2; *N*, cleaved nuclear forms of SREBP1 and SREBP2. (*D*) UT-59 does not inhibit secretion of S1P(ΔTM). On day 0, CHO/S1P(ΔTM) cells were set up in medium R at a density of 6×10^4 cells per well of a 48-well plate. On day 1, the medium was removed, cells were washed twice with 500 μL of PBS followed by addition of 200 μL of medium M containing one of the following reagents: UT-59 (indicated concentrations); BFA (2 μg/mL); 25-HC (2.5 μM); cholesterol/MCD complexes (30 μM). After incubation at 37 °C for 4 h, the medium and cells were collected and processed, and equal aliquots of the media and cell lysates were subjected to immunoblot analysis as described in *SI Appendix, Methods*. Chol., cholesterol. (*E*) UT-59 does not inhibit thapsigargin-induced transport of ATF6 from ER to Golgi. On day 0, SV-589 cells were set up in medium B at a density of 4×10^5 cells per well of a six-well plate. On day 1, the medium was removed and replaced with 2 mL of fresh medium B. The cells were then transfected with 1 μg of pTK-HSV-ATF6 using the FuGENE6 transfection agent according to the manufacturer's protocol. On day 2, the transfection medium was removed, cells were washed once with 3 mL of PBS, followed by addition of 2 mL of medium B supplemented with 25 μg/mL ALLN along with the indicated reagents at the following concentrations: thapsigargin (1 μM); UT-59 (30 μM); cholesterol/MCD complexes (30 μM). After incubation at 37 °C for 4 h, the medium was removed, cells were washed with 3 mL of PBS, harvested, and equal aliquots of cell lysates were subjected to immunoblot analysis as described in *SI Appendix, Methods*. *P*, precursor form of HSV-ATF6; *N*, cleaved nuclear form of HSV-ATF6; Chol., cholesterol.

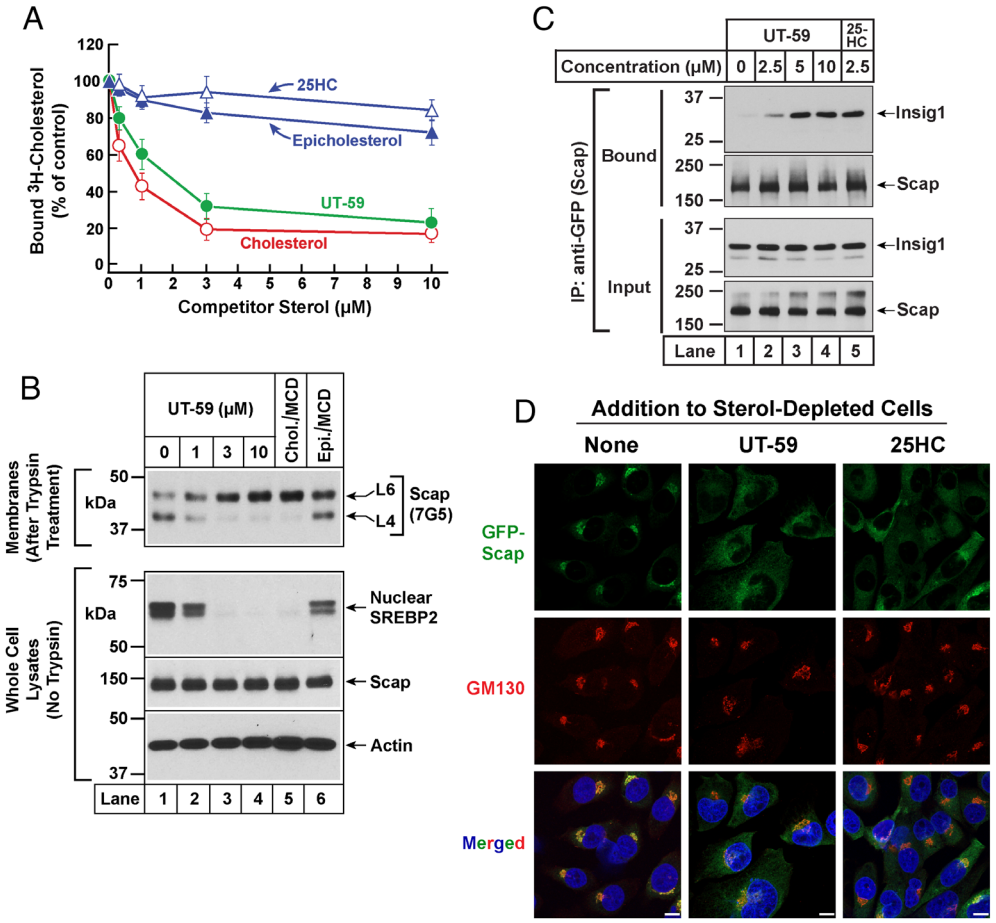

Fig. 4. UT-59 binds to Scap and changes its conformation, promoting Scap's binding to Insig, which blocks ER-to-Golgi transport of Scap. (*A*) Competitive binding to Scap's L1. Each reaction, in a final volume of 200 μL of buffer A with 0.004% NP-40 and 0.002% FC-13, contained 0.2 μg of His_6-Scap(L1)-FLAG, 1 μg of BSA, 150 nM [^{3}H]cholesterol (110,000 dpm/pmol), and varying concentrations of the indicated unlabeled sterol. After incubation for 4 h at 4 °C, bound [^{3}H]cholesterol was measured as described in *SI Appendix, Methods*. The 100% control value, determined in the absence of competitor, was 493 fmol/tube. Each data point represents the average of three assays and error bars represent the SE. When not visible, error bars are smaller than the size of the symbols. (*B*) Conformation change in Scap. On day 0, CHO-K1 cells were set up in medium K at a density of 1 × 10^6 cells per 10-cm dish. On day 2, the medium was removed, cells were washed twice with 10 mL of PBS followed by addition of 10 mL of cholesterol-depleting medium Q. After incubation at 37 °C for 1 h, the medium was removed, cells were washed twice with 10 mL of PBS followed by addition of 10 mL of medium P containing one of the following reagents: UT-59 (indicated concentrations); cholesterol/MCD complex (50 μM); epicholesterol/MCD complex (50 μM). After incubation at 37 °C for 3 h, the medium was removed, cells were washed twice with 10 mL of PBS, harvested, and processed for trypsin cleavage assays and immunoblot analysis as described in *SI Appendix, Methods*. Arrows in the *Top* panel denote two protease-protected fragments, L6 and L4. Chol., cholesterol; Epichol., epicholesterol. (*C*) Co-immunoprecipitation. On day 0, Scap-deficient SRD-13A cells were set up in medium L at a density of 7 × 10^5 cells per 10-cm dish. On day 2, media was removed and replaced with 10 mL of medium K. The cells were then transfected with 2 μg of pTK-Insig1-6xMyc together with 0.5 μg of pCMV-EGFP-Scap using X-tremeGENE HP transfection agent according to the manufacturer's protocol. On day 4, the transfection medium was removed, cells were washed with 10 mL of PBS, followed by addition of 10 mL of cholesterol-depleting medium Q. After incubation at 37 °C for 1 h, the medium was removed, cells were washed with 10 mL of PBS, followed by addition of medium P supplemented with the indicated concentrations of either UT-59 or 25-HC. After incubation at 37 °C for 3 h, the medium was removed, cells were washed twice with 10 mL of PBS, harvested, and processed for co-immunoprecipitation assays and immunoblot analysis as described in *SI Appendix, Methods*. (*D*) ER-to-Golgi transport. On day 0, CHO/pGFP-Scap cells were set up in medium N at a density of 6 × 10^4 cells per well of a 24-well plate where each well contained a 12-mm round glass coverslip. On day 1, the medium was removed, cells were washed twice with 500 μL of PBS followed by addition of 500 μL of cholesterol-depleting medium Q. After incubation at 37 °C for 1 h, the medium was removed, cells were washed twice with 500 μL of PBS, followed by addition of 500 μL of medium P supplemented with 5 μL of DMSO without or with either UT-59 (5 μM) or 25-HC (2.5 μM). After incubation at 37 °C for 3 h, the medium was removed, cells were washed twice with 500 μL of PBS, and the coverslips were removed and processed for microscopy analysis as described in *SI Appendix, Methods*. (Scale bar, 10 μm.)

luminal Loop 1 (*SI Appendix*, Fig. S1). As shown in the *Top* panel of Fig. 4*B*, in the absence of cholesterol, we detected two bands between the 50-kDa and 37-kDa markers (lane 1). The slower migrating band is generated by cleavage in Scap's Loop 6 and has been designated as "L6." The faster migrating band is generated by cleavage in Loop 4 at either lysine 378 or arginine 380 (*SI Appendix*, Fig. S1) and has been designated as "L4." Upon addition of increasing concentrations of UT-59, we observed a reduction in the amount of the L4 band and a commensurate increase in the amount of the L6 band (lanes 2 to 4), identical to what was observed upon cholesterol addition (lane 5). No such changes in the L6 and L4 bands were detected upon addition of epicholesterol (lane 6), which does not bind Scap's L1. Analysis of cell lysates before trypsin addition (but after sterol treatment) showed that UT-59 and cholesterol suppressed the processing of SREBP2 to its cleaved nuclear form, whereas epicholesterol did not affect processing (second panel, Fig. 4*B*), as would be expected based on the specificity of these compounds for binding Scap's L1.

The results so far show that UT-59 mimics cholesterol in binding to Scap's L1 and triggering a conformational change in Scap. We next performed a co-immunoprecipitation assay to assess whether UT-59 would promote the binding of Scap to Insig in the same manner as sterols. We transfected Scap-deficient SRD-13A cells with plasmids encoding Myc-tagged Insig1 and EGFP-tagged Scap. The transfected cells were first depleted of sterols, after which we incubated the cells with either UT-59 or 25HC. The

membranes were then solubilized and the EGFP-tagged Scap was isolated using GFP-Trap magnetic beads. The magnet-bound proteins were blotted with anti-Scap or anti-Myc (for Insig1). In the absence of sterols, very little Insig1 was detected and this increased as increasing amounts of UT-59 were added to the cells (lanes 1 to 4, Fig. 4*C*). The amount of Insig1 bound to Scap in the presence of UT-59 was similar to that detected when the cells were incubated with 25HC, which is known to promote Scap/Insig complex formation (lane 5, Fig. 4*C*). We then assessed whether UT-59-induced binding of Scap to Insig would retain Scap in the ER in a similar manner as sterols. For this experiment, we used a previously described Scap-deficient cell line that stably expresses a version of Scap that is fused to GFP (49). The cells were first depleted of sterols, then treated with either UT-59 or 25HC, and subjected to fluorescence microscopy analysis. In the absence of sterols, the GFP signal from Scap was concentrated in discrete punctae that also stained for GM130, indicating that Scap was in the Golgi stacks (left column, Fig. 4*D*). In contrast, when treated with UT-59, the GFP signal from Scap showed a lacy distribution distinct from the GM130 signal, consistent with retention in the ER (middle column, Fig. 4*D*). Similar ER retention was observed when the cells were treated with 25HC, which is known to suppress ER-to-Golgi transport of Scap (right column, Fig. 4*D*). These results support a model in which UT-59 suppresses transport of the Scap/SREBP complex from the ER to Golgi by binding directly to Scap's cholesterol-binding site, triggering a conformational change that promotes binding to Insig, which prevents Scap's incorporation into COPII transport vesicles.

Insigs Are Required for Mediating UT-59's Inhibition of Scap/SREBP Transport. We conducted three additional experiments to define the role of Insigs in mediating UT-59's suppression of Scap/SREBP transport. First, we tested the effects of UT-59 in SRD-15 cells, a mutant version of CHO-7 cells that lacks both isoforms of Insig (50). When UT-59 was added to sterol-depleted wild-type CHO-7 cells (containing Insigs), it suppressed the processing of both SREBP1 and SREBP2 at concentrations of 3 μM and higher (lanes 1 to 5, *Left*, *SI Appendix*, Fig. S6*A*). This dose–response was consistent with our previous assays of UT-59's effects in diverse cell types (Fig. 3*C* and *SI Appendix*, Fig. S4). In contrast, UT-59 did not suppress processing of either isoform of SREBP in the Insig-deficient SRD-15 cells (lanes 1 to 5, *Right*, *SI Appendix*, Fig. S6*A*). As expected, 25HC, which blocks SREBP processing by binding to Insigs, promoting Insig/Scap complex formation and triggering the same conformational change in Scap as induced by cholesterol (38, 39), was unable to do so in Insig-deficient SRD-15 cells (compare lane 6 of *Left* and *Right*, *SI Appendix*, Fig. S6*A*). Second, we used the cell growth assay described in *SI Appendix*, Fig. S5*C* to test UT-59's effects in SRD-15 cells. While UT-59 and 25HC led to cell death in CHO-7 cells, they did not affect the growth of the Insig-deficient SRD-15 cells (*SI Appendix*, Fig. S6*B*), consistent with the inability of UT-59 or 25HC to suppress SREBP processing and lipid synthesis in cells lacking Insigs.

As a third test, we studied the effects of UT-59 on SREBP2 transport in Scap-deficient SRD-13A cells that were transfected with either WT Scap or mutant versions of Scap containing one of three point mutations that destroy its ability to bind Insigs (Y298C, L315F, or D443N) (*SI Appendix*, Fig. S1) (3). As expected, UT-59 suppressed the ability of WT Scap to mediate transport and processing of SREBP2 in a manner similar to 25HC (lanes 1 to 7, *SI Appendix*, Fig. S6*C*). In contrast, UT-59, as well as 25HC, were unable to block SREBP2 transport and processing in cells expressing any of the three mutant Scaps that do not bind Insigs (lanes 8 to 28, *SI Appendix*, Fig. S6*C*). Combined, these experiments establish an absolute requirement for Insigs in mediating UT-59's actions on Scap. Once UT-59 binds to Scap and changes Scap's conformation, the UT-59-bound Scap still needs to bind Insigs to be retained in the ER along with the SREBPs. In the absence of Insigs, UT-59 is no longer able to block SREBP transport. This failure of UT-59 is similar to the failure of cholesterol to block Scap-mediated transport of SREBPs in Insig-deficient cells (39, 50).

UT-59 Does Not Trigger Cholesterol Transport from PM to ER or Activate Smoothened in PMs. We carried out two additional experiments to rule out the effects of UT-59 on other cholesterol-mediated pathways. In one study, we evaluated the effect of UT-59 on intracellular cholesterol trafficking. Most of the cell's cholesterol is located in the plasma membrane (PM), whereas the Scap/SREBP machinery is located in the ER. Continuous flow of cholesterol from the PM to the ER alerts the Scap/SREBP machinery of increases in cellular cholesterol, leading to reduced synthesis of cholesterol and other lipids (51, 52). While the competition assays in Fig. 4*A* suggest that there is a direct interaction between UT-59 and Scap's L1, we considered the possibility that UT-59 may also facilitate the movement of cholesterol from the PM to the ER, which would then bind to Scap and indirectly contribute to UT-59's effect of blocking SREBP transport. We tested this possibility by assaying the activity of acyl-CoA:cholesterol acyltransferase (ACAT), an ER enzyme that esterifies ER cholesterol and thus reports on cholesterol delivery to the ER (53). In the experiment described in *SI Appendix*, Fig. S7*A*, we lowered the sterol content of CHO-K1 cells by incubation in lipoprotein-poor LPDS along with compactin, an inhibitor of cholesterol biosynthesis. We then incubated the cells with UT-59, LDL, or 25HC together with [^{14}C]oleate for 3 h, after which the cells were processed for measurement of cholesteryl [^{14}C]oleate. No increase in cholesteryl [^{14}C]oleate formation was detected after UT-59 addition (*SI Appendix*, Fig. S7 *A*, *Top*). In contrast, the addition of LDL, whose cholesterol content is liberated and delivered to the ER (51), or 25HC, which triggers the rapid internalization of cholesterol from the PM to the ER (54), resulted in a dramatic increase in cholesteryl [^{14}C]oleate formation (*SI Appendix*, Fig. S7 *A*, *Top*). The formation of [^{14}C]triglycerides was similar for all treatments indicating that UT-59 did not affect the cellular entry and subsequent transport of [^{14}C]oleate to the ER (*SI Appendix*, Fig. S7 *A*, *Bottom*). These results suggest that UT-59 does not directly trigger ACAT activity or lead to movement of significant amounts of cholesterol to the ER.

In another study, we evaluated the effect of UT-59 on the Hedgehog signaling pathway that controls the activation of the GLI transcription factor family that modulates developmental growth pathways in animals (55). Activation of the GLI transcription factors is orchestrated by the binding of cholesterol to the extracellular domain of Smoothened (SMO), a G-protein-coupled receptor in the PM that transmits the Hedgehog signal to the nucleus. Inasmuch as UT-59 is a cholesterol-mimic in the context of binding to Scap's L1, we wondered whether UT-59 would bind SMO and activate the GLI transcription factors as cholesterol does. We tested this hypothesis in the experiment described in *SI Appendix*, Fig. S7*B*, where we incubated NIH 3T3 cells (a mouse fibroblast cell line) with UT-59, cholesterol, or Sonic Hedgehog (SHH) for 20 h, after which the cells were processed for mRNA analysis. No increase in Gli1 mRNA was detected after UT-59 addition (*SI Appendix*, Fig. S7 *B*, *Top*). In contrast, addition of cholesterol or SHH, a potent SMO agonist, led to a ~5-fold and 80-fold induction of Gli1 mRNA levels, respectively

(*SI Appendix*, Fig. S7 *B*, *Top*). While UT-59 had very little effect on Gli1 mRNA levels, it did lead to the reduction of mRNA levels of HMG-CoA reductase, a known SREBP2 gene target, to a similar degree as cholesterol (*SI Appendix*, Fig. S7 *B*, *Bottom*). While this is by no means an exhaustive analysis of all cellular pathways that are affected by cholesterol, these results further highlight the specificity of UT-59 for Scap.

Comparison of UT-59 to Other Reported Inhibitors of SREBP Processing. As described earlier, other groups have described five small molecules that inhibit SREBP processing, but their specificity had not been rigorously evaluated. We carried out a rigorous comparison of the potency and specificity of these five molecules—fatostatin, betulin, xanthohumol, lycorine, dipyridamole—to UT-59 (the chemical structures of all compounds are shown in the *Left* panel of *SI Appendix*, Fig. S8*A*). We compared their potency in assays measuring the suppression of SREBP1 processing in sterol-depleted human fibroblasts and their specificity in assays measuring the secretion of S1P(ΔTM) from a hamster cell line. UT-59 suppressed the processing of SREBP1 to its nuclear form at a concentration of 3 μM (lane 4 in first panel, *SI Appendix*, Fig. S8*A*), while having no effect on ER-to-Golgi transport and secretion of S1P(ΔTM) at all concentrations tested (lanes 1 to 6 in second panel, *SI Appendix*, Fig. S8*A*). Apart from xanthohumol, all of the other compounds were much less potent than UT-59 at suppressing SREBP1 processing (lanes 1 to 6 of immunoblots in *SI Appendix*, Fig. S8*A* and quantifications in *SI Appendix*, Fig. S8*B*). Moreover, all of the other compounds also blocked secretion of S1P(ΔTM) to a much higher degree than UT-59 (lanes 1 to 6 of immunoblots in *SI Appendix*, Fig. S8*A* and quantifications in *SI Appendix*, Fig. S8*C*). Xanthohumol had the strongest effects on blocking secretion of S1P(ΔTM) (*SI Appendix*, Fig. S8 *A* and *C*), consistent with its reported off-target activity in binding COPII proteins (24). We then used the competition assay described in Fig. 1*C* to measure the ability of these compounds to compete for the binding of [^{3}H]cholesterol to His$_6$-Scap(L1)-FLAG. As shown in *SI Appendix*, Fig. S8*D*, UT-59 competed with [^{3}H]cholesterol for binding to His$_6$-Scap(L1)-FLAG to a similar degree as unlabeled cholesterol. In contrast, none of the other five molecules that inhibit SREBP processing to some degree competed for the binding of [^{3}H]cholesterol to His$_6$-Scap(L1)-FLAG. As a control, 25HC, a sterol that does not bind Scap, did not compete for the binding of [^{3}H]cholesterol binding in this experiment. We conclude that UT-59 is the only compound, to date, that 1) selectively blocks Scap/SREBP transport without blocking the general process of ER-to-Golgi transport and 2) shows high specificity in competing for cholesterol binding to Scap's Loop1.

UT-59 Blocks SREBP Processing in the Mouse Liver. In a final set of experiments, we assessed the ability of UT-59 to block SREBP processing in the livers of mice. To be useful in vivo, UT-59 must survive in the circulation and enter the target tissue. To this end, we introduced UT-59 into mice by three different methods—intravenous, intraperitoneal (IP), and oral gavage—and then assessed its stability in plasma and in the target tissue, namely the liver (*SI Appendix*, *Methods*). All three delivery methods resulted in accumulation of UT-59 in the liver after 90 min. However, in all cases, the compound was rapidly cleared over the next few hours, with less than 10% remaining in the liver after 4 h. The IP method resulted in the highest concentration of UT-59 in the liver after 4 h and was therefore used as the dosing method to evaluate the in vivo effects of UT-59 in blocking SREBP processing.

We first focused on the effects of UT-59 on processing of SREBP-1c in the mouse liver. The essential role of Scap in insulin-mediated activation of SREBP-1c was established in previous studies where deletion of Scap in the liver reduced lipid synthesis in insulin-resistant *ob/ob* mice (56). Hepatic Scap deficiency also prevented the activation of SREBP-1c in response to refeeding following fasting (57). Here, we tested whether UT-59 would block SREBP-1c processing in response to refeeding. As shown in the schematic in *SI Appendix*, Fig. S9*A*, we provided mice ad libitum access to food (chow diet, see *SI Appendix*, *Methods*) for 6 h, after which the food was removed. After 18 h of fasting, food was again provided to the mice for 6 h, and this fasting/refeeding cycle was repeated for 3 d. On the fourth day, at the end of the feeding period, the food was removed, and the mice were intraperitoneally injected with increasing concentrations of UT-59. After 3 h, the mice were killed, and their livers were analyzed for proteins by immunoblot analysis. As shown in *SI Appendix*, Fig. S9*B*, the robust cleavage of SREBP1 in the four vehicle-treated mice (lanes 1 to 4) was blocked by UT-59 in a dose-dependent manner (lanes 5 to 16). The immunoblot signals in *SI Appendix*, Fig. S9*B* for the nuclear forms of SREBP1 from the vehicle-treated group (lanes 1 to 4) and the group treated with 30 mg/kg of UT-59 (lanes 9 to 12) were quantified and the results are shown in *SI Appendix*, Fig. S9*C* (Exp. 1, blue symbols). We repeated this experiment in four independent experiments on different days and the quantification of the immunoblots from these repeat studies is shown in *SI Appendix*, Fig. S9*C* (Exps. 2 to 5, differently colored symbols). In all cases, a dose of 30 mg/kg of UT-59 reduced SREBP1 cleavage by >70%.

We next explored the effects of UT-59 on processing of SREBP2 in the mouse liver. As shown in the schematic of *SI Appendix*, Fig. S9*D*, we provided mice ad libitum access to food containing lovastatin, an inhibitor of cholesterol synthesis that induces the activation of SREBP2 in the liver (58). On the eighth day, the food was removed, and the mice were intraperitoneally injected with increasing concentrations of UT-59. After 3 h, the mice were killed, and their livers were analyzed for proteins by immunoblot analysis. As shown in *SI Appendix*, Fig. S9*E*, the robust cleavage of SREBP2 in the four vehicle-treated mice (lanes 1 to 4) was blocked by UT-59 in a dose-dependent manner (lanes 5 to 16). The immunoblot signals in *SI Appendix*, Fig. S9*E* for the nuclear forms of SREBP2 from the vehicle-treated group (*lanes 1 – 4*) and the group treated with 60 mg/kg of UT-59 (*lanes 13 – 16*) were quantified and the results are shown in *SI Appendix*, Fig. S9*F* (Exp. 1, blue symbols). We repeated this experiment two more times on different days and the quantification of the immunoblots from these repeat studies is shown in *SI Appendix*, Fig. S9*F* (Exps. 2 and 3, differently colored symbols). In all cases, a dose of 60 mg/kg of UT-59 reduced SREBP2 cleavage by ~75%. Combined, these results provide a proof-of-principle that UT-59, a specific Scap inhibitor, can block SREBP processing in animals and sets the stage for testing the effects of specifically blocking the synthesis of fatty acids, triglycerides, and cholesterol in animal models of lipid dysregulation.

Discussion

Our current studies have identified UT-59 as a specific inhibitor of Scap that binds to Scap's cholesterol-binding site and blocks activation of SREBPs. Upon binding, UT-59 triggers the same conformational change in Scap as that induced by cholesterol and promotes the binding of Scap to Insigs, which retains Scap in the ER (Fig. 4). Inasmuch as Scap is bound to SREBPs, UT-59's halting of the transport of Scap also halts the transport of SREBPs from ER to Golgi and their subsequent proteolytic activation, leading to a reduction in the expression of lipogenic genes and lipid synthesis (Fig. 3*C* and *SI Appendix*, Figs. S3 and S4). None

of five previously reported small molecule inhibitors of SREBP processing—fatostatin, betulin, xanthohumol, lycorine, and dipyridamole—bind to Scap's cholesterol-binding site in the manner that UT-59 does (*SI Appendix*, Fig. S8*D*), highlighting the specificity of UT-59 as a cholesterol-mimicking inhibitor of Scap.

The identification of UT-59 was made possible by an unconventional screening strategy based on recent insights into how Scap senses membrane cholesterol. The cholesterol-binding domain in Scap, which controls SREBP activation, is not located in the transmembrane core of the protein, but rather in a loop of Scap (L1) that projects out of the membrane but can somehow dip into the membrane to bind cholesterol at the membrane surface (*SI Appendix*, Fig. S1) (4, 7, 36). The accessibility of cholesterol at the membrane surface is controlled by its formation of complexes with membrane phospholipids and reflects the chemical activity of cholesterol (34, 59). A growing body of evidence suggests that the manner in which Scap detects accessible cholesterol at the ER membrane surface shares similarities with how other cholesterol sensors, including bacterial cholesterol-binding toxins such as ALO, detect this form of cholesterol (33, 60). Using these insights, we developed a high-throughput screen to identify ALO-binding small molecules and found that one of these ALO binders, UT-59, also bound Scap and blocked SREBP activation in the exact same manner as cholesterol (Figs. 2–4).

Owing to its cholesterol-mimicking properties, one may expect UT-59 to share some structural similarities with cholesterol. As shown in Fig. 3*A*, UT-59 has a core diaryl urea scaffold modified with an ethyl ester at one end (*Right* side) and with a cyclobutyl-substituted oxadiazole ring at the other end (*Left* side). This molecular arrangement of UT-59 appears to bear little similarity to cholesterol, whose tetracyclic steroid nucleus scaffold is modified with an iso-octyl sidechain on one end and a hydroxyl group at the other end (Fig. 3*A*). How do such different molecules bind to the same site in both a bacterial soluble cholesterol-sensing protein (ALO) and a human membrane-bound cholesterol-sensing protein (Scap)? Unfortunately, there are no structures of either Scap's L1 or ALO bound to cholesterol or UT-59. Insofar as UT-59 is much more soluble than cholesterol, obtaining structures of ALO or Scap bound to UT-59 may be more feasible. We are currently pursuing such efforts to understand how cholesterol sensors recognize cholesterol.

In addition to providing structural insights into how cholesterol changes Scap's conformation, UT-59 promises to be a useful resource for in vitro studies such as determining the sensitivity of cancer cell lines to inhibition of the Scap/SREBP pathway. UT-59 could also be valuable for testing the effects of blocking Scap-mediated processing and the synthesis of cholesterol, fatty acids, and triglycerides in animal models of lipid dysregulation. Our initial proof-of-principle analysis suggests that the prospects of UT-59 functioning in vivo are bright. In these studies where mice were treated with UT-59 for 3 h, we observed a marked reduction in the insulin-induced activation of SREBP-1c (*SI Appendix*, Fig. S9 *A–C*) and the lovastatin-induced activation of SREBP-2 (*SI Appendix*, Fig. S9 *D–F*) in their livers. However, UT-59's short half-life in the circulation and livers of mice (~3 h) limited its use in more advanced in vivo studies. Having surmounted the first challenge of developing a specific Scap inhibitor, we hope to generate analogs of UT-59 with improved pharmacokinetic properties that will survive in the blood and liver for longer time periods and allow us to better study the effects of Scap inhibition on decreasing lipid synthesis in the liver and lowering levels of cholesterol and triglycerides in blood.

Once analogs or new scaffolds with improved bioavailability become available, we will need to examine the toxicity in vivo of these potential drug candidates. In the current experiments where we intraperitoneally injected UT-59 (*SI Appendix*, Fig. S9), we observed no overt toxicity, albeit after a short treatment time of only 3 h. In previous studies of liver-specific Scap knockout in mice (56) or liver-specific siRNA knockdown of Scap in mice, hamsters, and rhesus monkeys (56, 61), no overt deleterious effects were observed. However, two recent studies have shown toxicity due to ER stress when deletion of Scap in the liver of mice is combined with either deletion of PTEN, which drives constitutive signaling of the mTOR pathway (62), or administration of diets rich in fructose (63). Inasmuch as our screening strategy includes counter assays that eliminate candidates that cause ER stress (Fig. 3*E* and *SI Appendix*, Fig. S5*A*), our inhibitors would avoid this side effect.

Another potential concern is that potent, bioavailable Scap inhibitors would inhibit Scap in tissues other than the liver. Special attention will need to be paid to the gastrointestinal tract, since a previous study showed that deletion of Scap in the mouse intestine caused acute toxicity (64). Although the intestinal damage was severe in these Scap-deficient homozygotes, no overt toxicity was observed in Scap-deficient heterozygotes (65). We would hope that Scap will not require complete pharmacological inhibition to achieve the desired metabolic effects in the liver—in much the same way that statins achieve their desired LDL-lowering effect without completely inhibiting hepatic mevalonate formation (66). If inhibitors with different chemical scaffolds can be generated, this may lead to compounds with a favorable therapeutic index, which will allow in vivo assessments of blocking lipid and lipoprotein synthesis. If successful, this approach could open the door to developing therapeutic leads for diseases of lipid dysregulation such as coronary artery disease, fatty liver disease, and certain types of cancer.

Methods

The hemolysis assays that underpin the basis of the screen were carried out with red blood cells (RBCs) from fresh rabbit blood (Innovative Research; Novi, MI) that were isolated and resuspended in ice-cold buffer C as described previously (34). Dose–curve analysis of the ability of sterols and other small molecules to inhibit hemolysis by His_6-ALO was carried out in a large-volume format in 1.7 mL microcentrifuge tubes. Each reaction, in a final volume of 50 μL of buffer A, contained 1 nM of His_6-ALO and varying amounts of the indicated sterols solubilized in DMSO [final concentration of DMSO in each reaction tube was 4% (v/v)]. After incubation for 1 h at room temperature, 450 μL of rabbit erythrocytes (isolated and resuspended in buffer C as described in *SI Appendix, Methods*) was added to each reaction mixture. After incubation for 10 min at room temperature, the extent of hemolysis was quantified as described previously (34) by measuring the release of hemoglobin (absorbance at 540 nm). The amount of hemoglobin released after treatment with 1% (w/v) Triton X-100 detergent was used as the positive control (100% value). High-throughput analysis of the ability of each of the compounds in the UTSW screening library to inhibit hemolysis by His_6-ALO, experimental models, buffers, and media used in this study, sources of commercially available reagents, procedures for generating all other reagents, and step-by-step descriptions of all assays and their reproducibility, are described in detail in *SI Appendix, Methods*.

Data, Materials, and Software Availability. All study data are included in the article and/or *SI Appendix*.

ACKNOWLEDGMENTS. We thank Mike Brown and Joe Goldstein for their encouragement, advice, and critical reading of the manuscript. We also thank Steve Young, Russell Debose-Boyd, Jay Horton, Jin Ye, and members of our laboratory for their critical review of the manuscript and for helpful discussions throughout this project. We are grateful to Lisa Beatty, Ijeoma Dukes, Camille Harry, Shomanike Head, Leticia Esparza, Alex Hatton, Breanna Rhea, and Alyssa Ayala for assistance with cell culture studies; Xiaoyu Wang, Noelle Williams, and the resources and expertise of UTSW's Preclinical Pharmacology Core for assistance

with determining the pharmacokinetic properties of UT-59; Chieu Nguyen, Myra Mak, and Brianna Wilson for excellent technical assistance with all the studies; and Nancy Heard for figure preparation. This project was supported by the NIH (HL160487 and AI158357 to A.R.; and GM118082 to R.R.), the Welch Foundation (I-1793 to A.R.), and the Leducq Foundation (19CVD04 to A.R.). Some of the research reported in this study was supported by the UTSW NORC grant from the NIH (P30DK127984). We are also grateful for support from the UTSW Simmons Comprehensive Cancer Center (Grant #2P30CA142543) and the UTSW High Throughput Screening Core Facility (Grant #S10RR027805). J.C.S. is a recipient of a predoctoral National Research Service Award from the NIH (T32GM131963).

Author affiliations: [a]Department of Molecular Genetics, University of Texas Southwestern Medical Center, Dallas, TX 75390; [b]Department of Biochemistry, University of Texas Southwestern Medical Center, Dallas, TX 75390; [c]Department of Biochemistry, Stanford University School of Medicine, Stanford, CA 94305; and [d]Department of Medicine, Stanford University School of Medicine, Stanford, CA 94305

1. M. S. Brown, J. L. Goldstein, The SREBP pathway: Regulation of cholesterol metabolism by proteolysis of a membrane-bound transcription factor. *Cell* **89**, 331–340 (1997).
2. J. D. Horton, J. L. Goldstein, M. S. Brown, SREBPs: Activators of the complete program of cholesterol and fatty acid synthesis in the liver. *J. Clin. Invest.* **109**, 1125–1131 (2002).
3. M. S. Brown, A. Radhakrishnan, J. L. Goldstein, Retrospective on cholesterol homeostasis: The central role of scap. *Annu. Rev. Biochem.* **87**, 783–807 (2018).
4. Y. Zhang *et al.*, Direct demonstration that Loop1 of Scap binds to Loop7: A crucial event in cholesterol homeostasis. *J. Biol. Chem.* **291**, 12888–12896 (2016).
5. R. Yan *et al.*, A structure of human Scap bound to Insig-2 suggests how their interaction is regulated by sterols. *Science* **371** (2021).
6. R. Yan *et al.*, Structural basis for sterol sensing by Scap and Insig. *Cell Rep.* **35**, 109299 (2021).
7. D. L. Kober *et al.*, Scap structures highlight key role for rotation of intertwined luminal loops in cholesterol sensing. *Cell* **184**, 3689–3701.e3622 (2021).
8. A. Radhakrishnan, J. L. Goldstein, J. G. McDonald, M. S. Brown, Switch-like control of SREBP-2 transport triggered by small changes in ER cholesterol: A delicate balance. *Cell Metab.* **8**, 512–521 (2008).
9. S. Li, M. S. Brown, J. L. Goldstein, Bifurcation of insulin signaling pathway in rat liver: mTORC1 required for stimulation of lipogenesis, but not inhibition of gluconeogenesis. *Proc. Natl. Acad. Sci. U.S.A.* **107**, 3441–3446 (2010).
10. J. L. Owen *et al.*, Insulin stimulation of SREBP-1c processing in transgenic rat hepatocytes requires p70 S6-kinase. *Proc. Natl. Acad. Sci. U.S.A.* **109**, 16184–16189 (2012).
11. R. Loomba, S. L. Friedman, G. I. Shulman, Mechanisms and disease consequences of nonalcoholic fatty liver disease. *Cell* **184**, 2537–2564 (2021).
12. J. C. Cohen, J. D. Horton, H. H. Hobbs, Human fatty liver disease: Old questions and new insights. *Science* **332**, 1519–1523 (2011).
13. R. U. Svensson, R. J. Shaw, Lipid synthesis is a metabolic liability of non-small cell lung cancer. *Cold Spring Harb. Symp. Quant. Biol.* **81**, 93–103 (2016).
14. M. T. Snaebjornsson, S. Janaki-Raman, A. Schulze, Greasing the wheels of the cancer machine: The role of lipid metabolism in cancer. *Cell Metab.* **31**, 62–76 (2020).
15. X. Bian *et al.*, Lipid metabolism and cancer. *J. Exp. Med.* **218** (2021).
16. J. Ye *et al.*, ER stress induces cleavage of membrane-bound ATF6 by the same proteases that process SREBPs. *Mol. Cell* **6**, 1355–1364 (2000).
17. T. Murakami *et al.*, Signalling mediated by the endoplasmic reticulum stress transducer OASIS is involved in bone formation. *Nat. Cell Biol.* **11**, 1205–1211 (2009).
18. J. Ye, Transcription factors activated through RIP (regulated intramembrane proteolysis) and RAT (regulated alternative translocation). *J. Biol. Chem.* **295**, 10271–10280 (2020).
19. K. Marschner, K. Kollmann, M. Schweizer, T. Braulke, S. Pohl, A key enzyme in the biogenesis of lysosomes is a protease that regulates cholesterol metabolism. *Science* **333**, 87–90 (2011).
20. B. Antonny, R. Schekman, ER export: Public transportation by the COPII coach. *Curr. Opin. Cell Biol.* **13**, 438–443 (2001).
21. Y. Choi, Y. Kawazoe, K. Murakami, H. Misawa, M. Uesugi, Identification of bioactive molecules by adipogenesis profiling of organic compounds. *J. Biol. Chem.* **278**, 7320–7324 (2003).
22. S. Kamisuki *et al.*, A small molecule that blocks fat synthesis by inhibiting the activation of SREBP. *Chem. Biol.* **16**, 882–892 (2009).
23. W. Shao, C. E. Machamer, P. J. Espenshade, Fatostatin blocks ER exit of SCAP but inhibits cell growth in a SCAP-independent manner. *J. Lipid Res.* **57**, 1564–1573 (2016).
24. S. Miyata, J. Inoue, M. Shimizu, R. Sato, Xanthohumol improves diet-induced obesity and fatty liver by suppressing sterol regulatory element-binding protein (SREBP) activation. *J. Biol. Chem.* **290**, 20565–20579 (2015).
25. J. J. Tang *et al.*, Inhibition of SREBP by a small molecule, betulin, improves hyperlipidemia and insulin resistance and reduces atherosclerotic plaques. *Cell Metab.* **13**, 44–56 (2011).
26. Y. C. Lin, H. Y. Chen, C. P. Hsieh, Y. F. Huang, I. L. Chang, Betulin inhibits mTOR and induces autophagy to promote apoptosis in human osteosarcoma cell lines. *Environ. Toxicol.* **35**, 879–887 (2020).
27. Z. G. Zheng *et al.*, Discovery of a potent SCAP degrader that ameliorates HFD-induced obesity, hyperlipidemia and insulin resistance via an autophagy–independent lysosomal pathway. *Autophagy* **17**, 1592–1613 (2020), 10.1080/15548627.2020.1757955.
28. R. M. Esquejo *et al.*, Dipyridamole inhibits lipogenic gene expression by retaining SCAP-SREBP in the endoplasmic reticulum. *Cell. Chem. Biol.* **28**, 169–179.e167 (2021).
29. R. W. Bourdeau *et al.*, Cellular functions and X-ray structure of anthrolysin O, a cholesterol-dependent cytolysin secreted by Bacillus anthracis. *J. Biol. Chem.* **284**, 14645–14656 (2009).
30. R. K. Tweten, E. M. Hotze, K. R. Wade, The unique molecular choreography of giant pore formation by the cholesterol-dependent cytolysins of gram-positive bacteria. *Annu. Rev. Microbiol.* **69**, 323–340 (2015).
31. S. C. Feil, J. Rossjohn, K. Rohde, R. K. Tweten, M. W. Parker, Crystallization and preliminary X-ray analysis of a thiol-activated cytolysin. *FEBS Lett.* **397**, 290–292 (1996).
32. L. D. Nelson, A. E. Johnson, E. London, How interaction of perfringolysin O with membranes is controlled by sterol structure, lipid structure, and physiological low pH. *J. Biol. Chem.* **283**, 4632–4642 (2008).
33. A. Sokolov, A. Radhakrishnan, Accessibility of cholesterol in endoplasmic reticulum membranes and activation of SREBP-2 switch abruptly at a common cholesterol threshold. *J. Biol. Chem.* **285**, 29480–29490 (2010).
34. A. Gay, D. Rye, A. Radhakrishnan, Switch-like responses of two cholesterol sensors do not require protein oligomerization in membranes. *Biophys. J.* **108**, 1459–1469 (2015).
35. A. Radhakrishnan, L. P. Sun, H. J. Kwon, M. S. Brown, J. L. Goldstein, Direct binding of cholesterol to the purified membrane region of SCAP: Mechanism for a sterol-sensing domain. *Mol. Cell* **15**, 259–268 (2004).
36. M. Motamed *et al.*, Identification of luminal Loop 1 of Scap protein as the sterol sensor that maintains cholesterol homeostasis. *J. Biol. Chem.* **286**, 18002–18012 (2011).
37. A. J. Brown, L. P. Sun, J. D. Feramisco, M. S. Brown, J. L. Goldstein, Cholesterol addition to ER membranes alters conformation of SCAP, the SREBP escort protein that regulates cholesterol metabolism. *Mol. Cell* **10**, 237–245 (2002).
38. A. Radhakrishnan, Y. Ikeda, H. J. Kwon, M. S. Brown, J. L. Goldstein, Sterol-regulated transport of SREBPs from endoplasmic reticulum to Golgi: Oxysterols block transport by binding to Insig. *Proc. Natl. Acad. Sci. U.S.A.* **104**, 6511–6518 (2007).
39. L. P. Sun, J. Seemann, J. L. Goldstein, M. S. Brown, Sterol-regulated transport of SREBPs from endoplasmic reticulum to Golgi: Insig renders sorting signal in Scap inaccessible to COPII proteins. *Proc. Natl. Acad. Sci. U.S.A.* **104**, 6519–6526 (2007).
40. J. H. Zhang, T. D. Chung, K. R. Oldenburg, A simple statistical parameter for use in evaluation and validation of high throughput screening assays. *J. Biomol. Screen* **4**, 67–73 (1999).
41. Z. Wu, D. Liu, Y. Sui, Quantitative assessment of hit detection and confirmation in single and duplicate high-throughput screenings. *J. Biomol. Screen* **13**, 159–167 (2008).
42. D. Cheng *et al.*, Secreted site-1 protease cleaves peptides corresponding to luminal loop of sterol regulatory element-binding proteins. *J. Biol. Chem.* **274**, 22805–22812 (1999).
43. P. J. Espenshade, D. Cheng, J. L. Goldstein, M. S. Brown, Autocatalytic processing of site-1 protease removes propeptide and permits cleavage of sterol regulatory element-binding proteins. *J. Biol. Chem.* **274**, 22795–22804 (1999).
44. Y. Misumi *et al.*, Novel blockade by brefeldin A of intracellular transport of secretory proteins in cultured rat hepatocytes. *J. Biol. Chem.* **261**, 11398–11403 (1986).
45. Y. Pommier, Topoisomerase I inhibitors: Camptothecins and beyond. *Nat. Rev. Cancer* **6**, 789–802 (2006).
46. J. E. Metherall, J. L. Goldstein, K. L. Luskey, M. S. Brown, Loss of transcriptional repression of three sterol-regulated genes in mutant hamster cells. *J. Biol. Chem.* **264**, 15634–15641 (1989).
47. J. L. Goldstein, R. B. Rawson, M. S. Brown, Mutant mammalian cells as tools to delineate the sterol regulatory element-binding protein pathway for feedback regulation of lipid synthesis. *Arch. Biochem. Biophys.* **397**, 139–148 (2002).
48. Y. Gao, Y. Zhou, J. L. Goldstein, M. S. Brown, A. Radhakrishnan, Cholesterol-induced conformational changes in the sterol-sensing domain of the Scap protein suggest feedback mechanism to control cholesterol synthesis. *J. Biol. Chem.* **292**, 8729–8737 (2017).
49. A. Nohturfft, D. Yabe, J. L. Goldstein, M. S. Brown, P. J. Espenshade, Regulated step in cholesterol feedback localized to budding of SCAP from ER membranes. *Cell* **102**, 315–323 (2000).
50. P. C. Lee, N. Sever, R. A. Debose-Boyd, Isolation of sterol-resistant Chinese hamster ovary cells with genetic deficiencies in both Insig-1 and Insig-2. *J. Biol. Chem.* **280**, 25242–25249 (2005).
51. A. Das, M. S. Brown, D. D. Anderson, J. L. Goldstein, A. Radhakrishnan, Three pools of plasma membrane cholesterol and their relation to cholesterol homeostasis. *Elife* **3**, e02882 (2014).
52. R. E. Infante, A. Radhakrishnan, Continuous transport of a small fraction of plasma membrane cholesterol to endoplasmic reticulum regulates total cellular cholesterol. *Elife* **6**, e25466 (2017).
53. J. L. Goldstein, S. K. Basu, M. S. Brown, Receptor-mediated endocytosis of low-density lipoprotein in cultured cells. *Methods Enzymol.* **98**, 241–260 (1983).
54. D. B. Heisler *et al.*, A concerted mechanism involving ACAT and SREBPs by which oxysterols deplete accessible cholesterol to restrict microbial infection. *eLife* **12**, e83534 (2023).
55. J. H. Kong, C. Siebold, R. Rohatgi, Biochemical mechanisms of vertebrate hedgehog signaling. *Development* **146**, dev166892 (2019).
56. Y. A. Moon *et al.*, The Scap/SREBP pathway is essential for developing diabetic fatty liver and carbohydrate-induced hypertriglyceridemia in animals. *Cell Metab.* **15**, 240–246 (2012).
57. G. Liang *et al.*, Diminished hepatic response to fasting/refeeding and liver X receptor agonists in mice with selective deficiency of sterol regulatory element-binding protein-1c. *J. Biol. Chem.* **277**, 9520–9528 (2002).
58. I. Shimomura *et al.*, Cholesterol feeding reduces nuclear forms of sterol regulatory element binding proteins in hamster liver. *Proc. Natl. Acad. Sci. U.S.A.* **94**, 12354–12359 (1997).
59. H. M. McConnell, A. Radhakrishnan, Condensed complexes of cholesterol and phospholipids. *Biochim. Biophys. Acta* **1610**, 159–173 (2003).
60. A. Radhakrishnan, R. Rohatgi, C. Siebold, Cholesterol access in cellular membranes controls Hedgehog signaling. *Nat. Chem. Biol.* **16**, 1303–1313 (2020).
61. K. K. Jensen *et al.*, Dose-dependent effects of siRNA-mediated inhibition of SCAP on PCSK9, LDLR, and plasma lipids in mouse and rhesus monkey. *J. Lipid Res.* **57**, 2150–2162 (2016).
62. S. Kawamura *et al.*, Inhibiting SCAP/SREBP exacerbates liver injury and carcinogenesis in murine nonalcoholic steatohepatitis. *J. Clin. Invest.* **132**, e151895 (2022).
63. J. Y. Kim *et al.*, PIDDosome-SCAP crosstalk controls high-fructose-diet-dependent transition from simple steatosis to steatohepatitis. *Cell Metab.* **34**, 1548–1560.e1546 (2022).
64. M. R. McFarlane *et al.*, Scap is required for sterol synthesis and crypt growth in intestinal mucosa. *J. Lipid Res.* **56**, 1560–1571 (2015).
65. S. Rong, J. G. McDonald, L. J. Engelking, Cholesterol auxotrophy and intolerance to ezetimibe in mice with SREBP-2 deficiency in the intestine. *J. Lipid Res.* **58**, 1988–1998 (2017).
66. J. L. Goldstein, M. S. Brown, A century of cholesterol and coronaries: From plaques to genes to statins. *Cell* **161**, 161–172 (2015).